Data-driven damage mechanics: an outlook to failure

Gilles Pijaudier-Cabot, Julien Khoury

Computational Modelling of Concrete and Concrete Structures – Meschke, Pichler & Rots (Eds)

Data-driven damage mechanics: an outlook to failure

G. Pijaudier-Cabot and J. Khoury
Université de Pau et des Pays de l'Adour, CNRS, LFCR, Anglet, France

ABSTRACT: With the rapid advancements in experimental techniques and the growth in the amount of available data, especially when using digital image correlation and tomography, modelling is facing the challenge of transforming this enormous amount of knowledge into analytical equations that govern the material response. Classical constitutive equations may struggle to capture complex material responses, which is among the reasons why data driven approaches emerged. In this study, we apply a data-driven scheme to the modelling of failure of a quasi-brittle material such as concrete and discuss the difficulties induced when modelling localized failure. For the sake of simplicity, we consider a one-dimensional problem. Synthetic data sets are generated from a bi-linear damage model and exhibit strain softening. As expected, the one-dimensional example of a bar subjected to tension demonstrates that the obtained solutions are sensitive to the finite element discretization. A localization limiter is needed and the implementation of a non-local (integral) model circumvents the difficulty. There is, however, a notable observation in this case: optimal sets of strain, stress, and non-local history variable lie consistently outside the data set and do not converge within the data set upon mesh refinement. Several possibilities for solving this problem are considered, from the enlargement of the data set with non-local effects to the introduction of an additional constraint e.g., following the Lip-field approach. The latter method preserves locality of the constitutive response and it is found to be very easy to implement.

1 INTRODUCTION

In recent years, data-driven approaches have begun to replace traditional constitutive models. This change comes from two main factors: the limitations of classical equations and the growing amount of experimental data now available. Traditional (analytical) constitutive models have long been used to model quasi-brittle materials like concrete. However, simplifying the behavior of these heterogeneous materials into a set of equations often relies on strong assumptions. Data-driven approaches offer a promising way to get around these limitations by relying directly on raw material data. Kirchdoerfer et al. (Kirchdoerfer and Ortiz 2016) introduced a data-driven computational scheme in which material behavior is no longer represented through constitutive equations, but rather by a discrete cloud of data points—referred to as a data set. Their formulation aims to minimize the distance between admissible mechanical states, satisfying compatibility and equilibrium, and the available data points representing the material behavior.

The present work has two main objectives. The first is to implement this data-driven framework in the case of damage due to cracking. This study uses a bi-linear model with strain softening, interpreted through a continuum damage approach. This model is used to build the data set needed for the data-driven damage solver. Herein, the data set will be synthetic, not experimental. The second objective is to apply the data driven approach to the case of failure due to strain localization. Because there is no regularization involved in the computational model, mesh dependence is observed. Spatial correlations needed for regularization are not included in the data set defined point wise and the traditional difficulties involved in the failure of strain-softening materials are observed. We examine how this issue may be solved.

2 ELASTIC DATA-DRIVEN MODEL

Kirchdoerfer and Ortiz proposed a data-driven computational mechanics framework in which the material behavior is represented by a discrete set (or cloud) of stress–strain pairs, (ε, σ), instead of a constitutive equation (Kirchdoerfer and Ortiz 2016, Kirchdoerfer and Ortiz 2017). This collection of points, referred to as the data set E, can originate either from experimental measurements and/or multiscale simulation results. The central idea of this approach is to directly exploit the data set without involving any explicit constitutive equation to describe the material response.

DOI: 10.1201/9781003660026-75

We shall restrict the presentation to a one dimensional bar, but the foregoing analyses may be easily extended to a general 3D configuration. Consider a body occupying the domain $\Omega \subset \mathbb{R}^n$, *with* u representing the displacement field. The compatibility equation is expressed as:

$$\varepsilon(x) = \nabla u(x), \tag{1}$$

where $\varepsilon(x)$ denotes the strain at point x, and $\nabla\bullet$ stands for the gradient. The balance of linear momentum, in the absence of inertia, is given by:

$$\nabla \cdot \sigma(x) + b(x) = 0, \tag{2}$$

where $\sigma(x)$ denotes the stress and $b(x)$ the force per unit length of the bar at each point x, taken equal to 0 in the remaining for simplicity. The local mechanical state at $x \in \Omega$ is therefore defined by the stress–strain pair $(\varepsilon(x), \sigma(x))$, while the global mechanical state of the system, denoted by Z, encompasses all such local states within Ω.

The global state Z must satisfy both compatibility and equilibrium conditions, with material responses belonging to the data set E. In practice, however, the data set often lacks an admissible state that simultaneously fulfills these conditions (Conti, Müller, and Ortiz 2018). To address this limitation, Kirchdoerfer and Ortiz proposed identifying the admissible state that minimizes its distance to the data set, with the distance defined as:

$$F(Z,E) = \int_\Omega \min_{(\varepsilon',\sigma')\in E} \left[\frac{1}{2} C(\varepsilon(x) - \varepsilon')^2 + \frac{1}{2C}(\sigma(x) - \sigma')^2 \right] dx, \tag{3}$$

where $\varepsilon(x)$ and $\sigma(x)$ denote the local states that satisfy compatibility and equilibrium, while (ε', σ') represent the candidate states contained in the material data set E. C is is an arbitrary numerical parameter.

For numerical implementation, the domain Ω is discretized into m finite elements and n nodes. Each element e is associated with its own data set of stress–strain pairs, $E_e = (\varepsilon'_e, \sigma'_e)$ for $e = 1, \ldots, m$. Consequently, the continuous functional (3) is approximated in discrete form as:

$$F(Z,E) = \sum_{e=1}^{m} F_e(\varepsilon_e, \sigma_e), \tag{4}$$

With

$$F_e(\varepsilon_e, \sigma_e) = \min_{(\varepsilon'_e,\sigma'_e)\in E_e} \left(\frac{1}{2} C_e(\varepsilon_e - \varepsilon'_e)^2 + \frac{1}{2C_e}(\sigma_e - \sigma'_e)^2 \right) \tag{5}$$

where ε_e and σ_e denote the strain and stress corresponding to element e. The discrete compatibility is then given by:

$$\varepsilon_e = \sum_{i=1}^{n} B_{ei} u_i, \tag{6}$$

where u_i represents the displacement at node i $(i = 1, 2, \ldots, n)$, and B_{ei} is the strain–displacement matrix component describing the contribution of nodal displacement u_i to the strain within element e.

The discrete equilibrium condition is expressed as:

$$\sum_{e=1}^{m} w_e B_{ei}^T \sigma_e = f_i, \tag{7}$$

where f_i denotes the external force applied at node i, and w_e represents the volume associated with element e, defined as $w_e = A_e L_e$, with A_e and L_e corresponding to the cross-sectional area and length of element e, respectively.

Compatibility is directly introduced in (5) and equilibrium is enforced by modifying the functional with the help of Lagrange multipliers at each node η_i. This leads to the following constrained formulation:

$$\delta\mathbb{F}(u,\sigma,\eta) = \delta\left(\sum_{e=1}^{m} w_e F_e \left(\sum_{i=1}^{n} B_{ei} u_i \sigma_e \right) - \sum_{i=1}^{n} \left(\sum_{e=1}^{m} w_e B_{ei} \sigma_e - f_i \right) \eta_i \right) = 0 \tag{8}$$

Minimization of the functional with respect to u, σ, and η yields:

$$\frac{\delta\mathbb{F}}{\delta u_i} \Rightarrow \sum_{e=1}^{m} w_e C_e \left(\sum_{j=1}^{n} B_{ej} u_j - \varepsilon'_e \right) B_{ei} = 0 \tag{9a}$$

$$\frac{\delta\mathbb{F}}{\delta \sigma_e} \Rightarrow \frac{1}{C_e}(\sigma_e - \sigma'_e) = \sum_{i=1}^{n} \mathrm{B}_{ei} \eta_i \tag{9b}$$

$$\frac{\delta\mathbb{F}}{\delta \eta_i} \Rightarrow \sum_{e=1}^{m} w_e B_{ei} \sigma_e = f_i \tag{9c}$$

Together, Equations (9) define a coupled system in which the unknowns are the displacements, stresses, and Lagrange multipliers. Equations (9a,9c) are recast as follow using equation (9b):

$$\sum_{j=1}^{n} \left(\sum_{e=1}^{m} w_e C_e B_{ej} B_{ei} \right) u_j = \sum_{e=1}^{m} w_e C_e \varepsilon'_e B_{ei} \tag{10a}$$

$$\sum_{j=1}^{n}\left(\sum_{e=1}^{m} w_e C_e B_{ei} B_{ej}\right)\eta_j = f_i - \sum_{e=1}^{m} w_e B_{ei}\sigma'_e \quad (10b)$$

Given the set $(\varepsilon'_e, \sigma'_e)$ for each element, note that the above two equations form a linear system.

The aim is to identify, for each element, the local data point within the data set that best satisfies the compatibility and equilibrium equations. At the initial iteration ($k = 0$), each element is randomly assigned a stress–strain pair $(\varepsilon_e^{\prime(0)}, \sigma_e^{\prime(0)})$ from the data set. Solving Equations (10a) and (10b) then provides the corresponding displacements $u_i^{(0)}$ and Lagrange multipliers $\eta_i^{(0)}$. Using Equation (9b), the stresses $\sigma_e^{(0)}$ are computed, while the associated strains $\varepsilon_e^{(0)}$ are obtained from the displacement field. This defines an initial set of local states $(\varepsilon_e^{(0)}, \sigma_e^{(0)})$. In the subsequent iterations, denoted as (k), and for each element, we look for the optimal state $(\varepsilon_e^{\prime(k+1)}, \sigma_e^{\prime(k+1)})$ that minimizes the distance between the solution of equations (10a, 10b) and the data set:

$$\frac{1}{2}C_e\left(\varepsilon_e^{(k)} - \varepsilon_e^{\prime(k+1)}\right)^2 + \frac{1}{2C_e}\left(\sigma_e^{(k)} - \sigma_e^{\prime(k+1)}\right)^2$$

$$\leq \frac{1}{2}C_e\left(\varepsilon_e^{(k)} - \varepsilon'_e\right)^2 + \frac{1}{2C_e}\left(\sigma_e^{(k)} - \sigma'_e\right)^2 \quad (11)$$

where $(\varepsilon_e^{(k)}, \sigma_e^{(k)})$ denote the local states computed at iteration k, and $(\varepsilon_e^{\prime(k+1)}, \sigma_e^{\prime(k+1)})$ correspond to the closest point belonging to the data set at iteration $k+1$. The pairs $(\varepsilon'_e, \sigma'_e)$ represent all candidate data points in the material data set.

Convergence of the iterative procedure is achieved when $\varepsilon_e^{\prime(k+1)}, \sigma_e^{\prime(k+1)} = \left(\varepsilon_e^{\prime(k)}, \sigma_e^{\prime(k)}\right)$ for all elements $e = 1, 2, \ldots, m$.

3 DAMAGE DATA-DRIVEN APPROACH

Extending this computational method to damage requires several steps. We follow here the methodology described in (Eggersmann, Kirchdoerfer, Reese, Stainier, and Ortiz 2019).

The data set, as illustrated in Figure 1, is now represented in a space where the history variable that controls damage is added. This history parameter is assumed to be known, it is a function of the strain history if damage is controlled by strain, of the stress history if damage is controlled by the stress. The history parameter is an internal variable of the material in the sense that given its value and given an arbitrary strain, the stress is defined in a unique way according to the data set.

It is important to note that according to this data driven approach, a constitutive does exist. The state of the material is defined by a set of variables

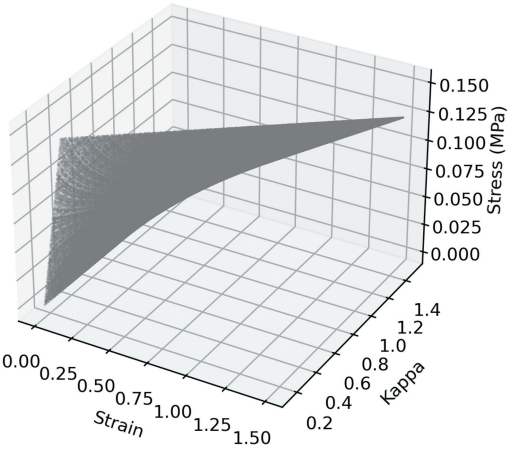

Figure 1. Example of material data set in the stress–strain–history parameter space.

(strain, history parameter), their conjugate quantites are also defined (stress and damage respectively), but the relationship between variables and their conjugate, which is the very definition of constitutive relations, is not defined analytically.

The system is discretized into n nodes and m elements. The material behavior at each element is characterized by a local state defined by the strain–stress–history triplet $\mathrm{E}_e = (\varepsilon_e, \sigma_e, \mathbb{K}_e)$ for $e = 1, \ldots, m$. As previously discussed, these local states must satisfy the compatibility and equilibrium conditions given in Equations (6) and (7). Moreover, the relationship between damage and the history parameter must be fulfilled:

$$f(\mathbb{K}_e) = D_e \quad (12)$$

where D_e denotes the damage associated with element e ($e = 1, 2, \ldots, m$).

Equilibrium is enforced through the Lagrange multipliers η_i, while the constraint on the history parameter is imposed using an additional set of Lagrange multipliers ξ_e. This leads to the following formulation:

$$\delta\mathbb{F}(u, \sigma, \eta, \xi) = \delta\left(\sum_{e=1}^{m} w_e Fe\left(\sum_{i=1}^{n} B_{ei} u_i \sigma_e\right)\right.$$

$$\left. - \sum_{i=1}^{n}\left(\sum_{e=1}^{m} w_e B_{ei}\sigma_e - f_i\right)\eta_i\right.$$

$$-\sum_{e=1}^{m}\left(f(\mathbb{K}_e)-D_e\right)\xi_e\Bigg)=0 \tag{13}$$

Minimization with respect to u, σ, η, and ξ yields:

$$\frac{\delta\mathbb{F}}{\delta u_i}\Rightarrow\sum_{e=1}^{m}w_eC_e\left(\sum_{j=1}^{n}B_{ej}u_j-\varepsilon'_e\right)B_{ei}=0 \tag{14a}$$

$$\frac{\delta\mathbb{F}}{\delta\sigma_e}\Rightarrow\frac{1}{C_e}\left(\sigma_e-\sigma'_e\right)=\sum_{i=1}^{n}B_{ei}\eta_i \tag{14b}$$

$$\frac{\delta\mathbb{F}}{\delta\eta_i}\Rightarrow\sum_{e=1}^{m}w_eB_{ei}\sigma_e=f_i \tag{14c}$$

$$\frac{\delta\mathbb{F}}{\delta\xi_e}\Rightarrow f(\mathbb{K}_e)=D_e \tag{14d}$$

Equations (15a) and (15b) are derived by combining Equations (14b) and (14c), and by manipulating Equation (14a), following the same procedure described in the previous section.

$$\sum_{j=1}^{n}\left(\sum_{e=1}^{m}w_eC_eB_{ej}B_{ei}\right)u_j=\sum_{e=1}^{m}w_eC_e\varepsilon'_eB_{ei} \tag{15a}$$

$$\sum_{j=1}^{n}\left(\sum_{e=1}^{m}w_eC_eB_{ei}B_{ej}\right)\eta_j=f_i-\sum_{e=1}^{m}w_eB_{ei}\sigma'_e \tag{15b}$$

The solver begins by specifying an initial state at time t and iteration $k=0$. Information from the previously converged step at $t-\delta t$, represented by the triplet $\left(\varepsilon_{e(t-\delta t)},\sigma_{e(t-\delta t)},\mathbb{K}_{e(t-\delta t)}\right)$, is used to generate these states. The history parameter is set to its value from the previous step, which is $\mathbb{K}'^{(0)}_{e(t)}=\mathbb{K}_{e(t-\delta t)}$. Strain and stress are defined following the same method to complete the initial triplet $(\varepsilon e(t)'^{(0)},\sigma'^{(0)}_{e(t)},\mathbb{K}'^{(0)}_{e(t)})$.

Using these initial local states, the global equilibrium and compatibility conditions are enforced by solving Equations (15a) and (15b), yielding the displacement field $u_i^{(0)}$ and the corresponding Lagrange multipliers $\eta_i^{(0)}$. From these quantities, the updated strain $\varepsilon^{(0)}_{e(t)}$ and stress $\sigma^{(0)}_{e(t)}$ fields are obtained using Equations (6) and (14b).

The equation defining the evolution of damage is then used to calculate the history parameter $\mathbb{K}^{(0)}_{e(t)}$ associated with the resulting stress-strain state $\varepsilon^{(0)}_{e(t)}$ and $\sigma^{(0)}_{e(t)}$. In current iteration (k), the material state is now fully defined by the triplet $\left(\varepsilon^{(k)}_{e(t)},\sigma^{(k)}_{e(t)},\mathbb{K}^{(k)}_{e(t)}\right)$. For each element, the optimal state in the data set $\left(\varepsilon^{'(k+1)}_{e(t)},\sigma^{'(k+1)}_{e(t)},\mathbb{K}^{'(k+1)}_{e(t)}\right)$. is updated through minimization of the following distance:

$$\begin{aligned}d=&\frac{1}{2}C_e\left(\varepsilon^{(k)}_{e(t)}-\varepsilon'^{(K+1)}_{e(t)}\right)^2+\frac{1}{2C_e}\left(\sigma^{(k)}_{e(t)}-\sigma'^{(k+1)}_{e(t)}\right)^2\\&+\frac{1}{2}C_e\left(\mathbb{K}^{(k)}_{e(t)}-\mathbb{K}'^{(K+1)}_{e(t)}\right)^2\le\frac{1}{2}C_e\left(\varepsilon^{(k)}_{e(t)}-\varepsilon'_e\right)^2\\&+\frac{1}{2C_e}\left(\sigma^{(k)}_{e(t)}-\sigma'_e\right)^2+\frac{1}{2}C_e\left(\mathbb{K}^{(k)}_{e(t)}-\mathbb{K}'_e\right)^2\end{aligned} \tag{16}$$

At this stage, two distinct scenarios may arise depending on the evolution of the history parameter.

- The first case occurs when $\mathbb{K}^{(k)}_{e(t)}>\mathbb{K}_{e(t-\delta t)}$, indicating that the material undergoes a change in its history variable. The minimization of the data-driven distance is therefore performed in the full three-dimensional strain–stress–history space, restricted to admissible points satisfying $\mathbb{K}>\mathbb{K}_{e(t-\delta t)}$. The current state $\left(\varepsilon^{(k)}_{e(t)},\sigma^{(k)}_{e(t)},\mathbb{K}^{(k)}_{e(t)}\right)$. is then projected onto this restricted data set to identify the optimal point $\left(\varepsilon'^{(K+1)}_{e(t)},\sigma'^{(K+1)}_{e(t)},\mathbb{K}'^{(K+1)}_{e(t)}\right)$.
- The second case arises when $\mathbb{K}_{e(t)}{}^{(k)}=_{e(t-\delta t)}$. In this situation, the admissible points are located in a two-dimensional stress–strain space at constant history parameter and damage, $\mathbb{K}=_{e(t-\delta t)}$ and $D=D_{e(t-\delta t)}$. The closest point satisfying these constraints is then selected as $\left(\varepsilon'^{(K+1)}_{e(t)},\sigma'^{(K+1)}_{e(t)},\mathbb{K}'^{(K+1)}_{e(t)}\right)$.

The history variable cannot decrease and configurations where $\mathbb{K}^{(k)}{}_{e(t)}<\mathbb{K}_{e(t-\delta t)}$ are not admissible. Convergence is reached when the assigned triplets remain unchanged between two successive iterations, i.e., when $\left(\varepsilon'^{(K+1)}_{e(t)},\sigma'^{(K+1)}_{e(t)},\mathbb{K}'^{(K+1)}_{e(t)}\right)=\left(\varepsilon'^{(K)}_{e(t)},\sigma'^{(k)}_{e(t)},\mathbb{K}'^{(K)}_{e(t)}\right)$ for all elements e = 1, 2,…, m. Once this condition is satisfied, the corresponding damage parameter D_e for each element is determined directly from the damage data set. The complete computational procedure is summarized in Algorithm 1.

Algorithm 1: Damage data-driven solver

Data: Local data sets $E_{e(t)}$ for $e = 1, \ldots, m$;
Applied loads $f_{i(t)}$, $i = 1, \ldots, n$
Result: Displacement $u_{i(t)}$, strain $\varepsilon_{e(t)}$, stress $\sigma_{e(t)}$, history parameter $\mathbb{K}_{e(t)}$
Initialize $k = 0$ at time t; **for** $e = 1$ **to** m **do**
  Randomly choose $(\varepsilon^{'(0)}_{e(t)}, \sigma^{'(0)}_{e(t)}, \mathbb{K}^{'(0)}_{e(t)})$ from the data set with $\mathbb{K}^{'(0)}_{e(t)} = \mathbb{K}_{e(t-\delta t)}$
repeat
  Solve for $u^{(k)}_{i(t)}$ and $\eta^{(k)}_{i(t)}$:

$$\sum_{j=1}^{n}\left(\sum_{e=1}^{m} w_e C_e B_{ej} B_{ei}\right) u_{j(t)} = \sum_{e=1}^{m} w_e C_e \varepsilon^{'(k)}_{e(t)} B_{ei},$$

$$\sum_{j=1}^{n}\left(\sum_{e=1}^{m} w_e C_e B_{ei} B_{ej}\right) \eta_{j(t)} = f_{i(t)} - \sum_{e=1}^{m} w_e B_{ei} \sigma^{'(k)}_{e(t)}.$$

  for $e = 1$ **to** m **do**
    $\varepsilon^{(k)}_{e(t)} = \sum_{i=1}^{n} B_{ei} u^{(k)}_{i(t)}$;
    $\sigma^{(k)}_{e(t)} = \sigma^{'(k)}_{e(t)} + C_e \sum_{i=1}^{n} B_{ei} \eta^{(k)}_{i(t)}$;
    $\mathbb{K}^{(k)}_{e(t)} = f(\varepsilon^{(k)}_{e(t)})$;
    if $\mathbb{K}^{(k)}_{e(t)} = \mathbb{K}_{e(t-\delta t)}$ **then**
      Choose $(\varepsilon^{'(k+1)}_{e(t)}, \sigma^{'(k+1)}_{e(t)}, \mathbb{K}^{'(k+1)}_{e(t)})$ closest to $(\varepsilon^{(k)}_{e(t)}, \sigma^{(k)}_{e(t)}, \mathbb{K}^{(k)}_{e(t)})$ from the 2D data set restricted to points satisfying $\mathbb{K} = \mathbb{K}_{e(t-\delta t)}$;
    else $\left(\mathbb{K}^{(k)}_{e(t)} > \mathbb{K}_{e(t-\delta t)}\right)$
      Choose $(\varepsilon^{'(k+1)}_{e(t)}, \sigma^{'(k+1)}_{e(t)}, \mathbb{K}^{'(k+1)}_{e(t)})$ closest to $(\varepsilon^{(k)}_{e(t)}, \sigma^{(k)}_{e(t)}, \mathbb{K}^{(k)}_{e(t)})$ from the 3D data set restricted to points satisfying $\mathbb{K} > \mathbb{K}_{e(t-\delta t)}$;
until;
if *all* $(\varepsilon^{'(k+1)}_{e(t)}, \sigma^{'(k+1)}_{e(t)}, \mathbb{K}^{'(k+1)}_{e(t)}) = (\varepsilon^{'(k)}_{e(t)}, \sigma^{'(k)}_{e(t)}, \mathbb{K}^{'(k)}_{e(t)})$ **then**
  $u_{i(t)} = u^{(k)}_{i(t)}$, $\varepsilon_{e(t)} = \varepsilon^{(k)}_{e(t)}$, $\sigma_{e(t)} = \sigma^{(k)}_{e(t)}$ and;
  Choose the damage parameter $D_{e(t)}$ related to the history parameter $\mathbb{K}^{(k)}_{e(t)}$ from the damage data set;
  exit
else
  $k \leftarrow k + 1$

4 BUILDING THE DATA SET

4.1 *Damage-based constitutive equations*

An isotropic scalar damage parameter driven by an equivalent tensile strain is used to model material degradation (Mazars and Pijaudier-Cabot 1989). The constitutive equation is defined by:

$$\sigma = E(1 - D).\varepsilon \tag{17}$$

where E is the Young's modulus of the undamaged material, D is a scalar damage parameter that ranges from 0 for undamaged materials to 1 for totally damaged materials, and ε and σ are the strain and stress respectively. The damage growth is controlled by the effective strain $\tilde{\varepsilon}$ defined as:

$$\tilde{\varepsilon} = \langle \varepsilon \rangle \tag{18}$$

where $\langle x \rangle_+$ denote the Macauley brackets. The limit of the reversible behavior is defined by:

$$f(\varepsilon) = \tilde{\varepsilon} - \mathbb{K} = 0 \tag{19}$$

with $\mathbb{K}$ being the history parameter. This parameter is used to track the records of damage that has already been triggered, and it is defined by:

$$\mathbb{K}(x,t) = \max_{(0,t)}\left(\tilde{\varepsilon}(x,t), \mathrm{K}_{tr0}\right) \tag{20}$$

where K_{tr0} is the damage threshold. If $d\varepsilon \leq 0$ and $f(\tilde{\varepsilon}) = 0$ or $f(\tilde{\varepsilon}) < 0$, the material will behave elastically. If $d\varepsilon > 0$ and $f(\tilde{\varepsilon}) = 0$, damage grows.

4.2 *Bi-linear data set*

The data set is constructed such that, under monotonic loading, the stress-strain response is:

$$\sigma(\varepsilon) = \begin{cases} (1-D)E\cdot\varepsilon & \text{for } \varepsilon \leq \mathbb{K} \\ E\cdot \mathrm{K}_{tr0} - H(\varepsilon - \mathrm{K}_{tr0}) & \text{for } \varepsilon > \mathbb{K} \end{cases} \tag{21}$$

H is the softening slope. A Young's modulus of $E = 1$ MPa is assumed. The elastic limit is defined at a strain value of $K_{tr0} = 0.15$, corresponding to a maximum stress of 0.15 MPa. Beyond this point, the nonlinear regime follows a softening slope of $H = -0.02\%$, and data are generated up to a maximum strain of $\varepsilon = 1.5$. Due to this gentle softening behavior, snap-back instability is avoided and computational results can be also compared to analytical solutions for checking purposes (see Ref. (Bažant 1976)). Figure 2 presents the resulting two-dimensional bi-linear data set.

The cloud of points is constructed using a strain increment of 1.10^{-4}, which serves as the main parameter controlling the data set's resolution. Each point defining the envelope curve is sequentially generated following the constitutive response described in Equation (21). The history parameter is assigned as the corresponding strain value at each of these locations (i.e., within the softening regime). The damage variable is then computed from the slope of the line connecting each point to the origin, which corresponds to a modulus of $E(1 - D)$.

Subsequently, internal points located along the red line or within the envelope curve are generated by keeping the damage and history parameters constant

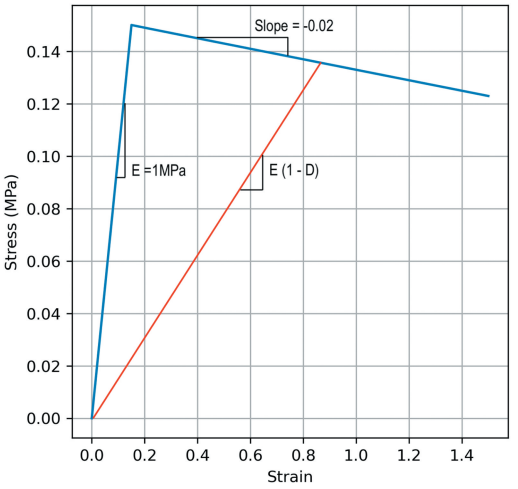

Figure 2. Stress–strain envelope for bi-linear data set.

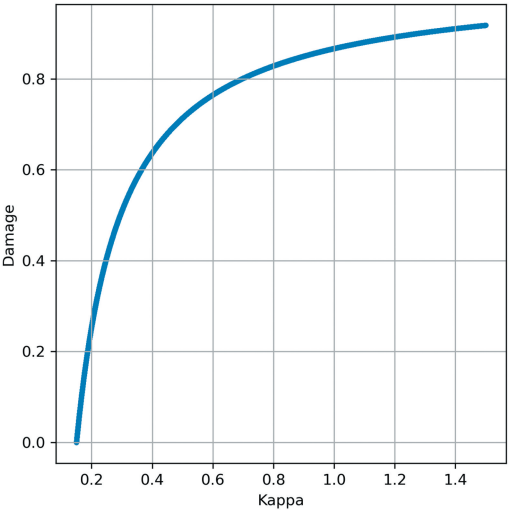

Figure 3. Damage evolution law.

while varying the strain according to the previously defined increment of 1.10^{-4}. This process yields a three-dimensional data set, as shown in Figure 1, with the corresponding evolution of damage, defined point wise and presented in Figure 3.

5 DATA-DRIVEN CALCULATIONS

The solver is tested on a one-dimensional bar fixed on one side and subjected to a tensile force on the other side. The bar has a length of 1050 mm with a cross-sectional area of 1 mm^2. It is discretized into n equal elements, yielding $n + 1$ nodes (Figure 4).

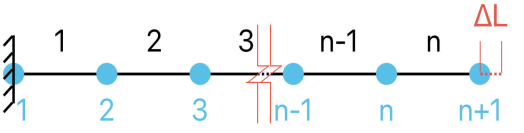

Figure 4. 1D bar with n elements and $n + 1$ nodes.

5.1 *Local damage calculations*

The bar is discretized into 5, 11, and 21 elements of equal size. A displacement increment of 10 mm is applied to load the bar up to 180 mm. Strain localization is triggered by placing a defect defined by a reduction of cross section of the central element by 10%, resulting in an area of 0.9 mm^2 instead of 1mm^2.

Figure 5 shows the load displacement responses for the several discretizations. As expected, the response is mesh dependent because strain localises in the central element only (in the defect). The data-driven local damage model inherits the classical drawbacks of local strain-softening formulations.

5.2 *non-local damage calculations*

In order to avoid mesh dependence due to strain localization, we switch to an analysis where the constitutive law is non-local (Pijaudier-Cabot and Bažant 1987). A spatial averaging of the parameters controlling damage is introduced. Localization issues should be mitigated, enabling computations to produce mesh-independent results.

The effective strain of the local model, previously defined in Equation (18), is replaced by a spatial average of the equivalent strain:

$$\bar{\varepsilon} = \frac{\int \psi \tilde{\varepsilon} dv}{\int \psi dv} \tag{22}$$

where ψ denotes a Gaussian function characterized by an internal length L_C, which is calibrated to represent the size of the region where strain localizes. The Gaussian function is:

$$\psi(x, s) = \exp\left(-\frac{(2\|x - s\|)^2}{L_C^2}\right) \tag{23}$$

where x denotes the spatial point at which the non-local averaging is evaluated, and s is a variable representing points in the domain.

It is important to emphasize that the effective strain, which governs the evolution of damage, is the only non-local quantity; stress, strain and the history parameter remain defined locally. The history parameter becomes defined as the maximum between a threshold value K_{tr0} and the spatially averaged equivalent strain. Introducing nonlocality does not

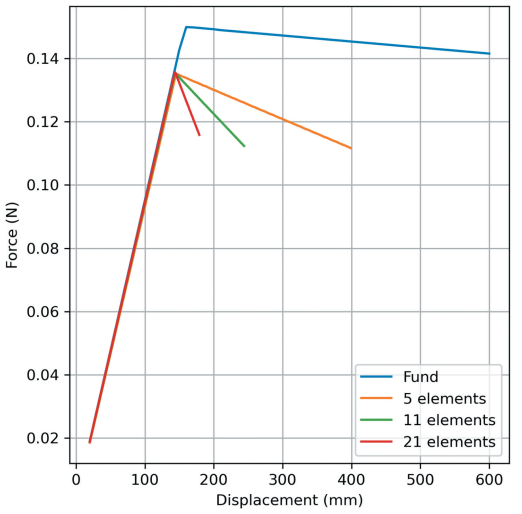

Figure 5. Force-displacement curves for the fundamental case and the different discretizations considered.

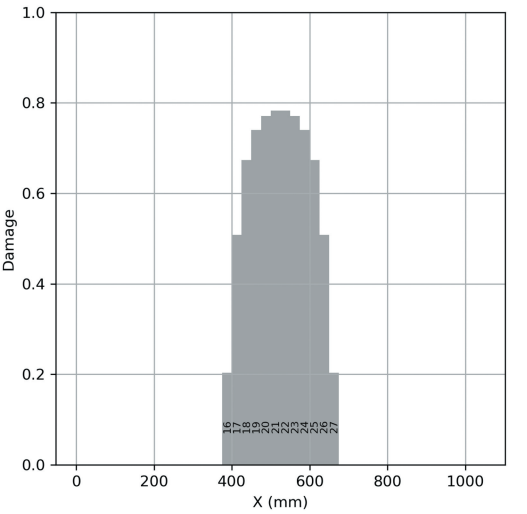

Figure 6. Results of the non-local damage solver for the 42-element bar with internal length $L_C = 30$ mm. Damage distribution in the bar at a total displacement of 245 mm (the numbers indicating element indices).

change the data set a priori, it is only the calculation of the history parameter which needs to be modified.

A 50 mm defect is introduced at the center of the previously considered bar by reducing the cross-sectional area of the affected elements to $0.9\,\text{mm}^2$. Fine discretizations are adopted, where elements are smaller than the internal length. The internal length is set as $L_c = 30\,\text{mm}$ and two discretizations are considered. The first discretization consists of a 42-element bar (each element being 25 mm long), while the second uses 105 elements (each 10 mm long). Same as in previous cases, the bar is subjected to tensile loading by fixing one end and imposing a displacement at the other. The corresponding results are presented in Figures (6, 7).

Due to the non-local formulation, damage is no longer confined to the defective elements but extends to their neighboring ones. The comparison between figure (6) and figure (7) shows that the damage profiles are quite similar. We can conclude that the data-driven computational technique, coupled with a non-local approach to damage, is capable of handling failure due to strain localization properly.

Upon a closer look, however, these results are not totally consistent. Figure (8) shows the stress-strain responses followed by each finite element during the calculation. Theoretically, the stress-strain responses for each element should belong to the data set, or close to the points of the data set within its resolution.

Outside the localization zone, elastic unloading is observed. Inside the localization zone, the response follows the stress–strain law, except for the two elements located at mid-length. An overshoot in the stress–strain response of these elements is observed: the stress exceeds the upper limit of the data set.

Upon further investigations, it turns out that this phenomenon is due to the presence of the defect. At the onset of localization, the local strain in the elements at the center of the bar (within the defect) is greater than the peak strain (assuming the bar is under a homogeneous state of strain). However, the non-local strain stays below the damage threshold because of non-local averaging. Hence the material response remains elastic. Unfortunately, there is no point in the data set that corresponds to such a response. In fact,

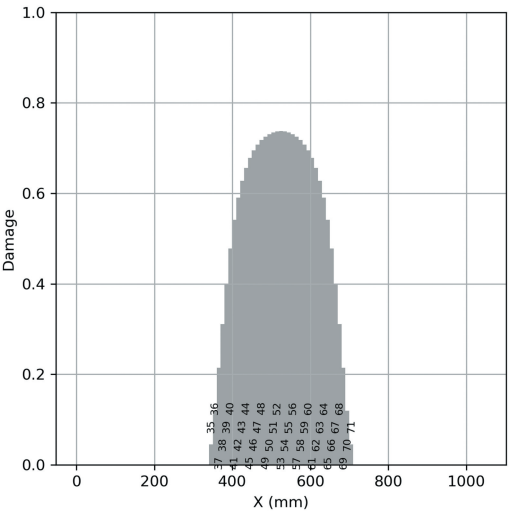

Figure 7. Results of the non-local damage solver for the 105-element bar with internal length $L_C = 30$ mm. Damage distribution in the bar at a total displacement of 245 mm (the numbers indicating element indices).

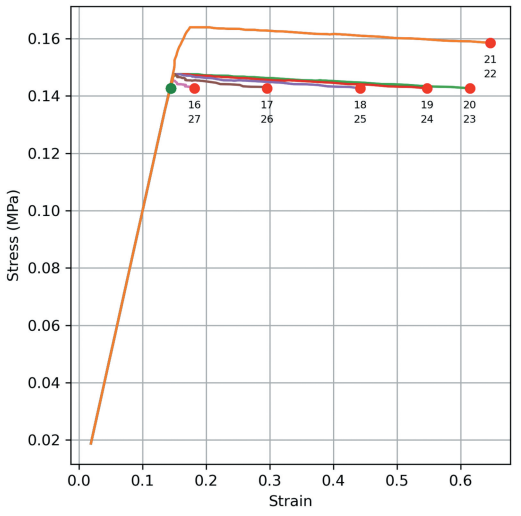

Figure 8. Stress-strain histories for within the finite element mesh showing an overshoot of the response for the two elements at the center of the localized zone.

the data set is restricted to stress–strain response for a bar under homogeneous deformation. The solver finds the closest point in the data set that satisfies equilibrium, meaning that the response of the element remains elastic, with a stress that is larger than the peak stress. This is perfectly admissible, it just points out that the data set is incomplete.

The data set used in the non-local formulation should be expanded to include additional key parameters that govern non-local effects. Constructing such a data set is challenging, as capturing non-locality effectively typically requires simulations across various geometries and internal lengths. In addition, it means also that the description of the material response needs to be enriched, e.g., by adding information from the non-local strain, otherwise given a state of strain and damage, there would be non unique stresses depending on the value of the non-local strain. Consequently, the functional to be minimised would need also to be enriched by adding the difference between the non-local strain computed from the FE calculation and the non-local strain belonging to the data set. This example shows clearly that extending the data driven approach to non-locality is not a straightforward.

5.3 *Lip-field damage computations*

In their 2021 study, Moës and Chevaugeon proposed a strategy to enforce Lipschitz regularity on the internal variable governing material softening as a means to prevent localization (Moës and Chevaugeon 2021). This approach preserves the local nature of the constitutive equations while ensuring regularization of the damage field through the introduction of a Lipschitz condition:

$$\frac{|D_a - D_b|}{|a - b|} \leq M \quad \forall a, b \in \Omega \tag{24}$$

where D_a and D_b denote the damage variables at positions a and b, $|a - b|$ represents the distance between the two points, M is the Lipschitz constant, and Ω is the domain. This condition limits the absolute value gradient of the damage profile, and of the strain profile as well.

The computational scheme that includes this constraint is only a slight modification of the local data-driven damage mechanics solver: the main modification arises in the stage where the history parameter ($\mathbb{K}^{(k)}_{e(t)}$) at iteration k is computed for all elements e (i.e., $e = 1, 2, \ldots, m$). In the local solver, the triplet $\varepsilon^{(k)}_{e(t)}, \sigma^{(k)}_{e(t)}, \mathbb{K}^{(k)}_{e(t)}$ is directly projected onto the data set. In contrast, the Lip-field solver introduces an intermediate step: the damage parameters $D^{(k)}_{e(t)}$ corresponding to each history parameter are first derived from the damage evolution law (see Figure 3). The Lipschitz-field regularization is then applied, resulting in a new set of damage parameters $D^{(k)}_{e(t)}$. Based on these regularized values, a new history parameter field, $\mathbb{K}^{(k)}_{e(t)}$ which satisfies the Lipschitz condition is reconstructed using the damage data set. We have now at iteration (k) a set of strain, stress and history variable which does not fully satisfies equilibrium because damage has been reduced due to the Lipschitz condition. Then, two possibilities arise: either new iterations are performed to arrive to sets within each finite element that comply with equilibrium and compatibility given the same trial state picked in the data set, or we use directly the computed sets, look for the new closest point in the data set, update the trial set from the data set, and perform a new global iteration. This second possibility has been implemented here, but it requires a modified projection scheme: for the elements where the Lipschitz condition is applied, the nearest point on the data set is looked at a constant value of the history parameter which results from the Lipschitz condition. When strain localization occurs, there is an infinite number of localized strain profile that are solution of the problem. In substance, the calculation is forced upon localization to follow a branch that complies with the Lipschitz condition in each finite element.

This formulation has been tested using the previously generated data sets on the same one-dimensional bar (1050 mm in length) subjected to tensile loading. The Lipschitz constant M, which governs the degree of regularization, is set to 3×10^{-3}. A 50 mm defect is considered to trigger localization (cross-sectional area reduced to 0.9 mm^2). The same discretizations used in the non-local case are adopted here, consisting of 42 and 105

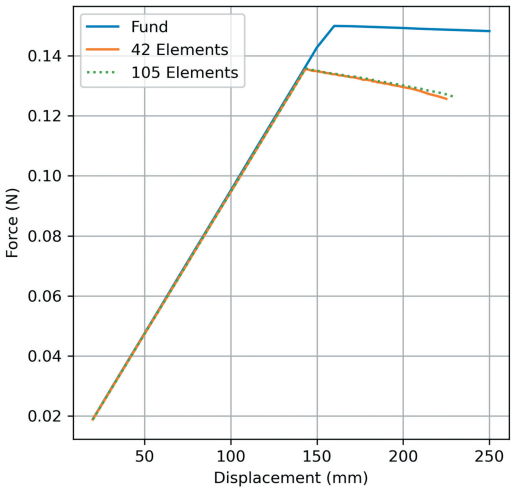

Figure 9. Force-displacement in 42- and 105-element bars with Lipschitz constant $M = 3 \times 10^{-3}$.

elements. The defect is assigned to the two central elements in the 42-element bar and to the five central elements in the 105-element bar.

Figure 9 compares the global force–displacement curves obtained from both meshes with the fundamental case where there is no localization (no defect). Figures 10 show the corresponding damage and strain distributions along the bar at the final time step, corresponding to a total displacement of 225 mm, for the two discretizations. Similar to the non-local solver, the Lip-field solver effectively eliminates mesh dependency. Because the constitutive equations are local, the difficulty encountered with the non-local approach are also avoided. There are no solutions in the stress-strain responses of every element that are not within the data set.

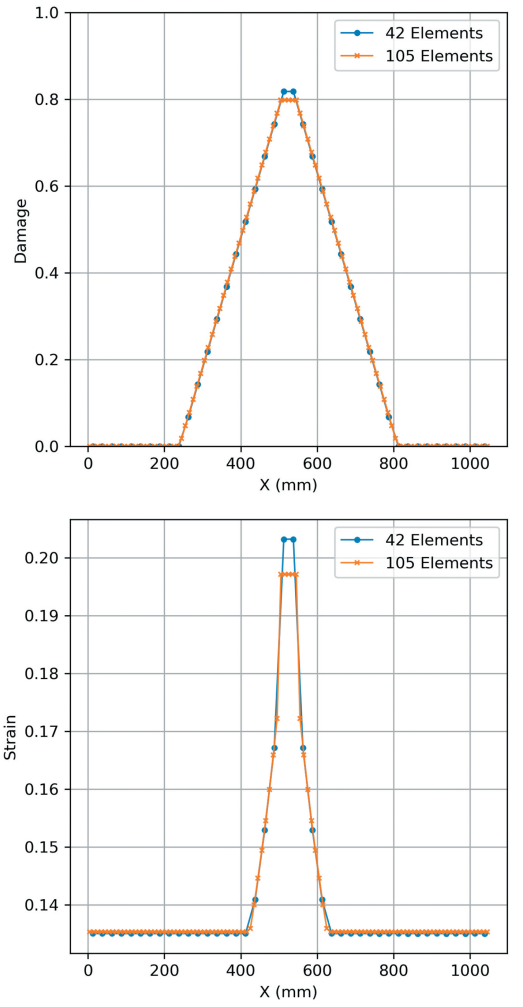

Figure 10. Damage (top) and strain (bottom) distributions in 42- and 105-element bars with Lipschitz constant $M = 3 \times 10^{-3}$.

6 CONCLUSIONS

In this work, a data-driven damage solver inspired by the approach proposed by Kirchdoerfer and Ortiz (Kirchdoerfer and Ortiz 2016, Kirchdoerfer and Ortiz 2017) is introduced. In this solver, the model parameters are considered as the material behavior variables. Thus, for damage models with a history parameter, the material behavior is defined through a data set of strain, stress, and history parameter $(\varepsilon, \sigma, \mathbb{K})$. This framework opens the door to material modeling without the need for explicit constitutive equations.

Three formulations were considered: local, non-local, and Lip-field solvers. The local solver inherited the limitations of classical local damage models, exhibiting strain and damage localization and mesh-dependent responses. The non-local formulation requires an enhancement of the data set, accounting for all possible non-local interactions. Its dimension needs to be increased also, a given state being defined by the stress, the strain, the non-local strain and the history parameter. The Lip-field formulation provides a practical alternative to maintain the local nature of the data set and turns out to be easily implemented in this data driven computational approach.

It should be pointed out finally that the present computational scheme does not suppress the need to define a constitutive model. In fact, it needs a clear definition of the state variables that control the material response and also an explicit definition of internal state variable as a function of the applied strain history in order to perform their computation during the calculations. The gain is that analytical expressions of the constitutive laws are not needed, instead data clouds of points are used.

ACKNOWLEDGMENTS

Partial financial support from the investissement d'avenir French programme (ANR-16-IDEX-0002), the European Union's Horizon 2020 research and innovation programme EDENE under the Marie Skłodowska-Curie grant agreement No 945416, and from the Communauté d'Agglomération Pau – Béarn – Pyrennées are gratefully acknowledged. This research was performed within the E2S hub Newpores supported jointly by Université de Pau et des Pays de l'Adour and Northwestern University.

REFERENCES

Bažant, Z. P. (1976). Instability, ductility, and size effect in strain-softening concrete. *Journal of the engineering mechanics division 102*(2), 331–344.

Conti, S., S. Müller, and M. Ortiz (2018). Data-driven problems in elasticity. *Archive for Rational Mechanics and Analysis 229*(1), 79–123.

Eggersmann, R., T. Kirchdoerfer, S. Reese, L. Stainier, and M. Ortiz (2019). Model-free data-driven inelasticity. *Computer Methods in Applied Mechanics and Engineering 350*, 81–99.

Kirchdoerfer, T. and M. Ortiz (2016). Data-driven computational mechanics. *Computer Methods in Applied Mechanics and Engineering 304*, 81–101.

Kirchdoerfer, T. and M. Ortiz (2017). Data driven computing with noisy material data sets. *Computer Methods in Applied Mechanics and Engineering 326*, 622–641.

Mazars, J. and G. Pijaudier-Cabot (1989). Continuum damage theory—application to concrete. *Journal of engineering mechanics 115*(2), 345–365.

Moës, N. and N. Chevaugeon (2021). Lipschitz regularization for softening material models: the lip-field approach. *Comptes Rendus. Mécanique 349*(2), 415–434.

Pijaudier-Cabot, G. and Z. P. Bažant (1987). Nonlocal damage theory. *Journal of engineering mechanics 113*(10), 1512–1533.